Visual Observation of CO_2 Foaming of Polypropylene-Clay Nanocomposites

KENTARO TAKI[1], TATSUNORI YANAGIMOTO[1], EITA FUNAMI[1], MASAMI OKAMOTO[2], *and* MASAHIRO OHSHIMA[1]

[1]*Department of Chemical Engineering*
Katsura Campus
Kyoto University, Kyoto 615-8510, Japan

[2]*Advanced Polymeric Materials Engineering*
Graduate School of Engineering
Toyota Technical Institute
Hisakata 2-12-1, Tempaku, Nagoya 468-8511, Japan

Using a newly developed high-pressure autoclave, which has two sapphire windows on the walls, we visually observed the batch physical foaming of polymer-clay nanocomposites to understand the effect of nano-sized clay on the initial stage of foaming. With CO_2 as a physical foaming agent, polypropylene-montmorillonite clay nanocomposites were foamed at 150°C. A high-speed digital camera with a microscope could observe the bubble nucleation and bubble growth behavior of the early stage of foaming *in situ*. The series of micrographs was analyzed in order to investigate the effect of clay content on bubble nucleation and growth. The experiments, together with CO_2-solubility and diffusivity data, show that the clay enhances bubble nucleation as a nucleation agent and retards the growth of bubbles at the early stage of foaming. Polym. Eng. Sci. 44:1004–1011, 2004.

INTRODUCTION

Several polymer-clay nanocomposites, such as polypropylene-montmorillonite (1–3), poly (lactic acid)-montmorillonite (4), and polyethylene-montmorillonite (5), have been developed. With their excellent clay-induced properties, these nanocomposites have attracted much attention. When a clay such as montmorillonite is introduced and mixed with a polymer, the mechanical strength of the composite is increased (6–8). The addition of clay also changes the gas permeability relative to the polymer (9, 10), and reduces the flammability (11). In the plastic foaming industries, the application of nanocomposites to microcellular foams is considered. Plastic foams, with bubble sizes less than 10 μm and bubble number density larger than 10^8~10^9 cm^{-3}, are called microcellular foams. A group at MIT proposed the concept of microcellular foam in the mid-1980s (12). When microcellular foam was introduced, it was claimed that, owing to the micro-sized bubbles, microcellular foam did not deteriorate the mechanical strength relative to non-foamed plastic. However, from the experience of making microcellular plastics with several neat resins, it was found that the mechanical strength of the microcellular foam was not improved as much as expected (13, 14). Therefore, there is an increasing expectation that microcellular foams of nanocomposites can maintain mechanical strength at desired levels.

There have been several studies on foaming of nanocomposites, such as polypropylene/clay nanocomposite (15), polycarbonate/clay nanocomposites (16), and polylactide/clay nanocomposites (17). From a Scanning Electron Microscope (SEM) micrograph of foamed polymer composites, it was speculated that the clay played the role of bubble-nucleating agent. As a result, the final bubble size was decreased and bubble density was increased. The previous studies also pointed out that the clay was oriented in the wall of bubbles along the stretched direction, which might enhance the mechanical strength of the foam (2, 15). Their entire conclusion comes only from static observations, i.e., SEM micrographs.

In the physical foaming process, an interaction exists between bubble nucleation and growth. When the number of bubble nuclei increases, the concentration of physical foaming agent (PFA) dissolved in the polymer matrix is suddenly reduced in the course of foaming.

Published online in Wiley InterScience (www.interscience.wiley.com).
DOI: 10.1002/pen.20093

The reduction in concentration suppresses the successive nucleation as well as the bubble growth because the nucleation is a function of dissolved PFA concentration, and the bubble growth is a function of mass transfer of PFA from the matrix to the bubbles. Furthermore, the bubble growth rate is not only a function of the number of nuclei but also of polymer viscosity and diffusivity of the PFA in the polymer.

To understand the complex mechanism of physical foaming, an *in-situ* observation of foaming is needed. Using a visual observation high-pressure cell, Taki *et al.* recently studied the dynamic behavior of bubble nucleation and growth in the batch physical foaming of polypropylene (18). They showed that micrographs of the early stage of foaming indicated that the mass transfer of PFA from the polymer matrix to bubbles dominates the bubble growth rate. In this study, visual observation of polypropylene/clay nanocomposite foaming is conducted by using a high-pressure cell so as to clarify the effect of clay in the polymer on the bubble nucleation and growth rates, i.e., the dynamic behavior of the early stage of foaming. Employing image-processing techniques, we analyzed the bubble nucleation and growth rates for different composites from the micrographs. Together with the solubility and diffusivity of PFA (CO_2) into the matrix polymer, the mechanism of nanocomposite foaming is investigated.

EXPERIMENTAL

Materials

The polypropylene-clay nanocomposites were prepared in the same way as in a previous study (15). The clay was montmorillonite and the matrix polymer was polypropylene, which was modified with 0.2% maleic anhydride. The composite was prepared by the method of melt intercalation. Three kinds of composite samples were prepared by changing the weight fraction of clay (2, 4, 7.5 wt%) in the composite. Hereafter, they are denoted as PPCN2, PPCN4 and PPCN7.5, respectively. For a reference, a sample of polypropylene modified with maleic anhydride, denoted as PPMA, was prepared. For the experimental setup, a sample sheet 0.2 mm in thickness was prepared by using a hot-press at 180°C, 10 MPa for 2 min, and it was punched to make disk-shaped samples 5 mm in diameter. To make a polymer foam by physical foaming, carbon dioxide (CO_2), the purity of which was 99%, was used as a PFA.

Measurements of Solubility and Diffusivity

The solubility and the diffusivity of carbon dioxide into the composites were measured by using a gravimetric technique for gas sorption measurements, i.e., the Magnetic Suspension Balance (MSB) (Bell Japan). The measurement scheme is detailed elsewhere (19). In order to correct the buoyancy effect on weighing, the Sanchez-Lacombe equation of state (20–22) was employed. The characteristic parameters of the equation of state were determined from pressure-volume-dependencies of PPMA and composites data obtained by a high-pressure GNOMIX PVT apparatus (Gnomix, Inc. USA) with an isothermal cooling procedure for the range of temperature from 90°C to 260°C and pressure from 10 MPa to 30 MPa. This dilatometer measures the volume changes of polymer samples as a function of temperature and pressure by using the confining fluid technique.

Visual Observation

Figure 1 shows a schematic diagram of the visual observation apparatus for batch physical foaming. It consists of a high-pressure cell, a gas-supply line, and a pump with a gas cylinder. The details of the cell can be found elsewhere (18).

The foaming experiments were performed with the following procedure. First, the cell was purged by PFA (e.g., CO_2) at a temperature of 40°C. Then, it was further heated to 180°C and kept at that temperature for 10 minutes to melt the crystals in the polymer. Following the heating, the cell was cooled to the set-point, 150°C, which was above the melting temperatures of all composite samples. When the temperature reached the set-point, the cell was pressurized by CO_2 to 13 MPa and kept at that temperature and pressure for one hour to dissolve CO_2 into the sample. The pressure and the temperature were maintained within ± 0.1°C and ± 0.05 MPa, respectively, around the set-point. After equilibrium was established, the pressure inside the cell was released to induce bubble nucleation. A pressure transducer monitored pressure changes every 0.1 sec. A high-speed CCD camera with a microscope took 100 pictures every second to observe the foaming phenomena. The start of picture-taking was synchronized with the moment when pressure in the cell was released. The largest magnification that the microscope could achieve was 750.

RESULTS AND DISCUSSION

Figure 2 shows the pressure profiles during the batch foaming experiments. The pressure in the cell was released from the saturation pressure, 13 MPa, by opening valve 2 in *Fig. 1*. Bubble nucleation occurred at around 2 or 3 sec after the pressure started descending. In order to evaluate the effect of clay on bubble nucleation and growth, the pressure profile has to be carefully controlled for every experiment to realize the same pressure conditions. The variability of the pressure profile at around 2 to 4 sec was less than 0.2 MPa among all the experiments.

Figure 3 shows a series of micrographs of PPMA and PPCN7.5 foaming. The magnification of the microscope is 150. Therefore, the frame size of the micrograph is 1.2 mm in height and 1.6 mm in width. The micrographs were taken every second. The micrographs of PPMA foaming are in the upper row and those of PPCN7.5 foaming are in the lower. They show the dynamic behavior of bubble nucleation and growth in the very early stage of physical foaming. The black dots are bubbles and the white part is the polymer matrix. The

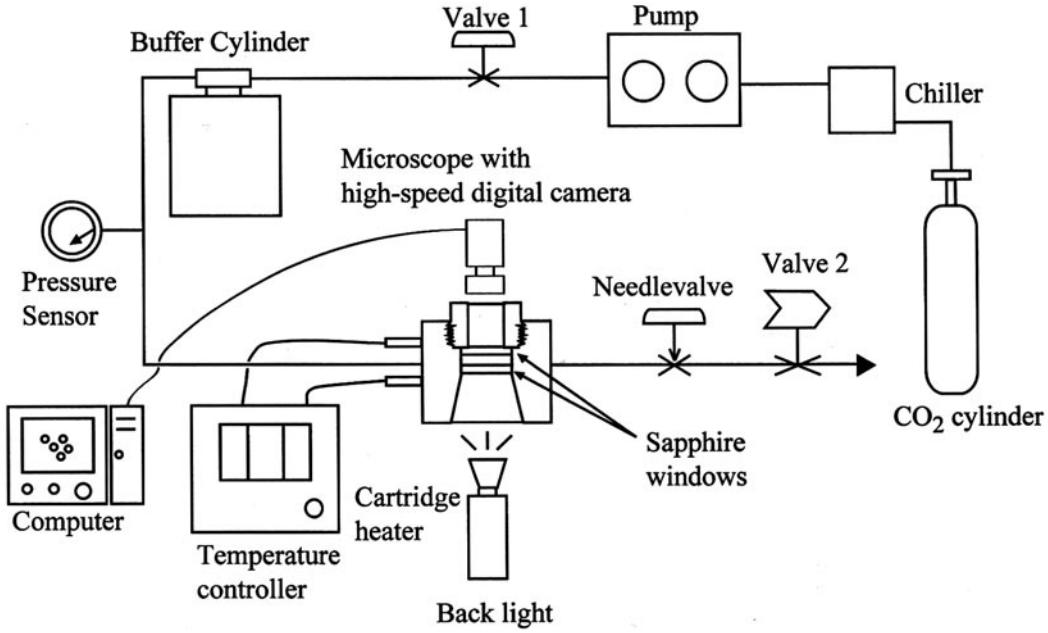

Fig. 1. Schematic diagram of visual observation apparatus.

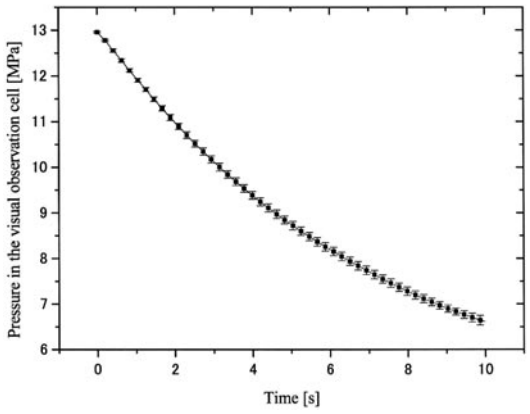

Fig. 2. Pressure profiles in the visual observation cell.

bubbles in the micrograph appear black because the bubbles reflect the light entering from the opposite-side window of the high-pressure cell. Both pictures clearly indicate that bubble nucleation and growth occur simultaneously.

A comparison of the micrographs of PPCN7.5 with those of PPMA found that the number of nucleated bubbles in PPCN7.5 foaming was much larger than that of PPMA, and the bubble growth rate in PPCN7.5 foaming was slower than that of PPMA. In order to evaluate the nucleation rate and the bubble growth rate in a quantitative way, the micrographs were analyzed by employing image-processing techniques. The bubble density is calculated by counting the number of bubbles observed in a micrograph and dividing the number by the volume of the micrograph (i.e., $1.2 \times 1.6 \times 0.2$ mm). *Figure 4* shows the temporal change in the bubble density at the PPMA and composite-foaming experiments. The density curve shows a sigmoid function shape at all composite-foaming experiments: having an induction time, the nucleation starts and the number of bubbles increases. At a certain moment, the nucleation is dramatically increased and then ceases. The value where the density curve reaches a steady state is called the final number density of the bubble. Because of the bubble coalescence, the final number density might not be equal to the bubble density of the final foam product. As can be seen in *Fig. 4*, the bubble nucleation rate and the final number density of the bubble become largest in the PPCN7.5 foaming. Although a distinct difference in bubble nucleation rate as well as in the final number density of the bubble could not be observed between PPCN2 and PPMA foaming, the nucleation rate and the final number density of the bubble increase as the weight fraction of the clay increases. Furthermore, the induction time becomes shorter as the clay content increases.

Since bubble nucleation is strongly correlated with the concentration of PFA dissolved in the polymer, the solubility and the diffusivity of CO_2 in composites were measured. *Figure 5* shows the pressure-volume-temperature dependency data of composites as well as that of PPMA. The characteristic parameters of the Sanchez-Lacombe equation of state were determined by fitting the equation to the data. The resulting parameters are listed in *Table 1*. The solubility was measured by a gravimetric method, i.e., magnetic suspension balance, where the weight changes of the sample caused by CO_2 sorption were measured in consideration of buoyancy. The PVT data was used for correcting the effect of buoyancy on the weight, i.e., calculating the specific volume

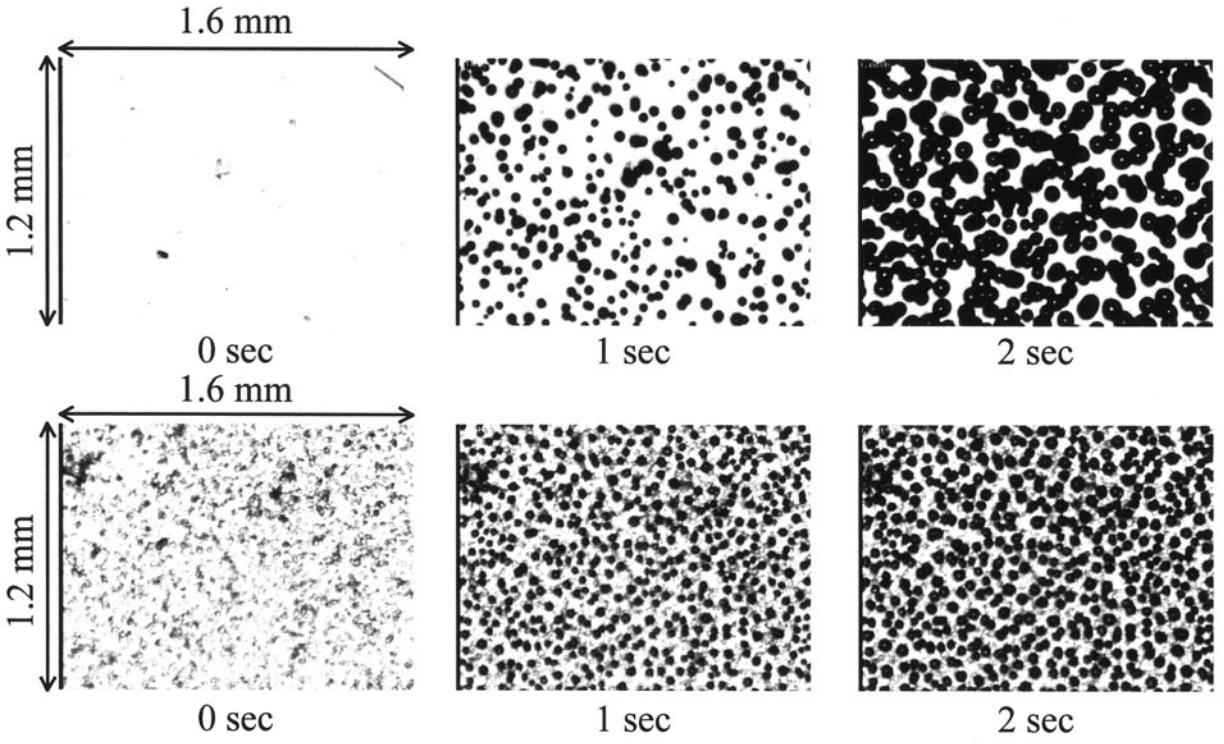

Fig. 3. Series of micrographs of physical foaming.

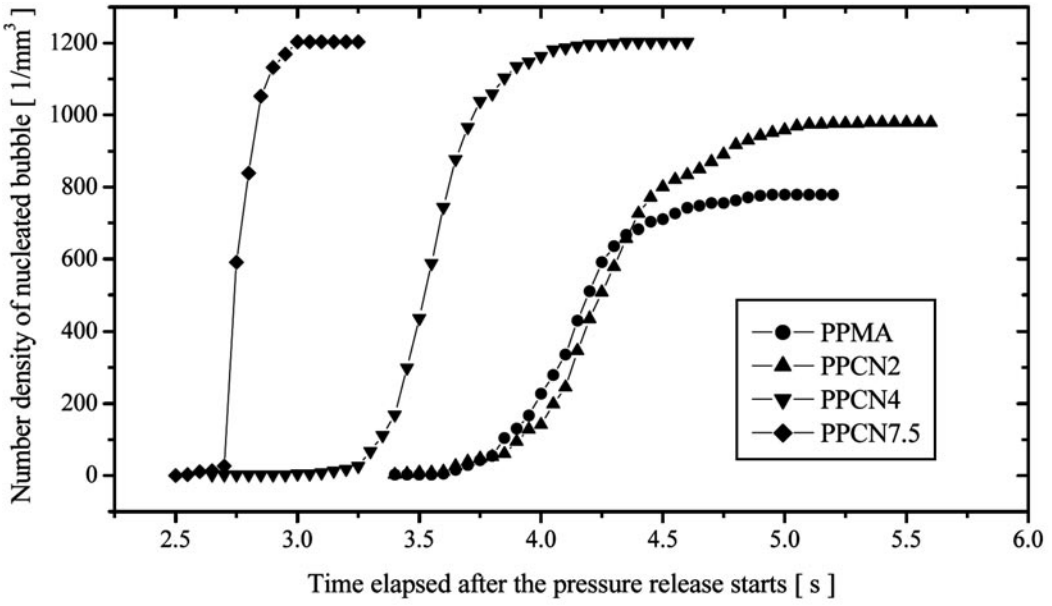

Fig. 4. Change in number density of nucleated bubble against time at PPMA and composite foaming.

change caused by CO_2 dissolution. The interaction parameters of the Sanchez-Lacombe equation of state for CO_2-polymer are also listed in *Table 1*. The details of the solubility measurement using the magnetic suspension balance can be found elsewhere (19).

Figure 6a shows the solubility of CO_2 into PPMA and composites. As can be seen, the solubility of CO_2 in composites as well as PPMA follows Henry's law. As the clay content increases, the solubility of CO_2 into composites decreases. Assuming that the dissolution of CO_2 into clay is negligible, the solubility of CO_2 into the polymer only is re-calculated. The resulting solubility is shown in *Fig. 6b*. The difference in solubility among the samples is small, which means that the concentration

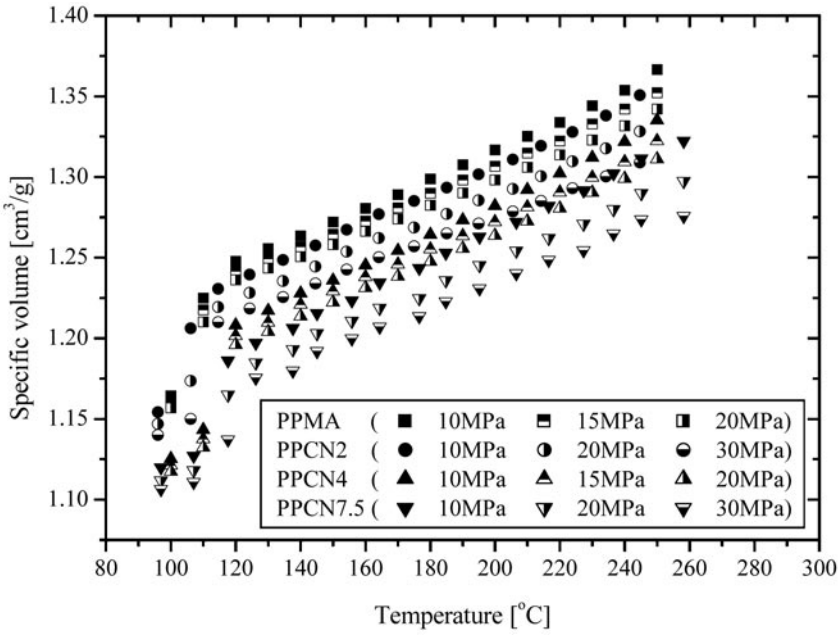

Fig. 5. Pressure-volume-temperature dependencies of PPMA and composites.

Table 1. Characteristic Parameters of Sanchez-Lacombe Equation for PPMA and Composites.

	Clay Content wt%	PPMA 0	PPCN2 2	PPCN4 4	PPCN7.5 7.5
ρ^*	kg/m^3	879.33	894.98	915.76	935.54
P^*	MPa	281.84	150.65	300.32	157.95
T^*	K	685.23	638.97	659.20	620.28
k_{12}	—	0.1055	0.1014	0.1211	0.1168

of CO_2 dissolved in the polymer alone is not changed by the clay content. Thus, the difference in nucleation rate among the samples is not caused by CO_2 concentration in the polymer. It could be caused by a clay-induced change in surface tension or the wetting factor between the clay and polymer interface. In other words, the clay acts as a bubble nucleating agent. This result supports the comments on the effect of clay described in other papers (15–17).

The bubble growth rate is quantified by measuring temporal change in the cross-sectional area of each bubble. *Figures 7a* and *b* show the changes in cross-sectional area at PPMA and PPCN7.5 foaming against the elapsed time after the pressure release started. Each line represents the average cross-sectional area of bubbles that emerged in the micrograph at the moment of time where the line started. Although some run-to-run error exists even for the cases where the pressure profiles were kept the same, most curves can be approximated by a linear function of the time. In this study, the slope of the straight line is used as an index for representing the growth rate of bubbles born at the time that the line starts; hereafter, it is called the representative average growth rate. The bubble growth rate could be determined by the mass transfer rate of

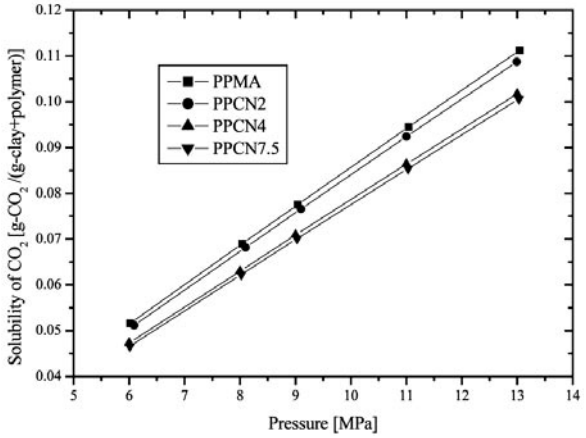

Fig. 6a. Solubility of CO_2 into PPMA and composites of whole sample.

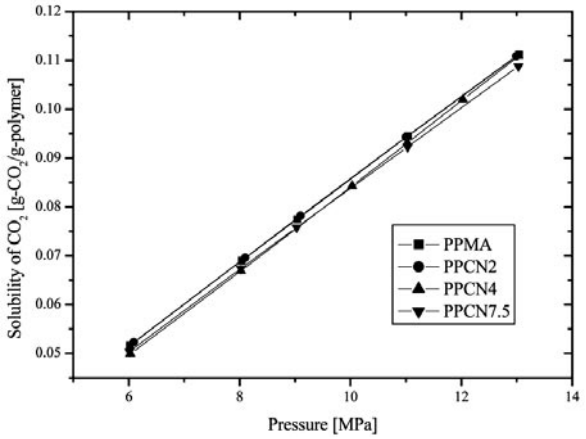

Fig. 6b. Solubility of CO_2 into PPMA and composites of polymer matrix.

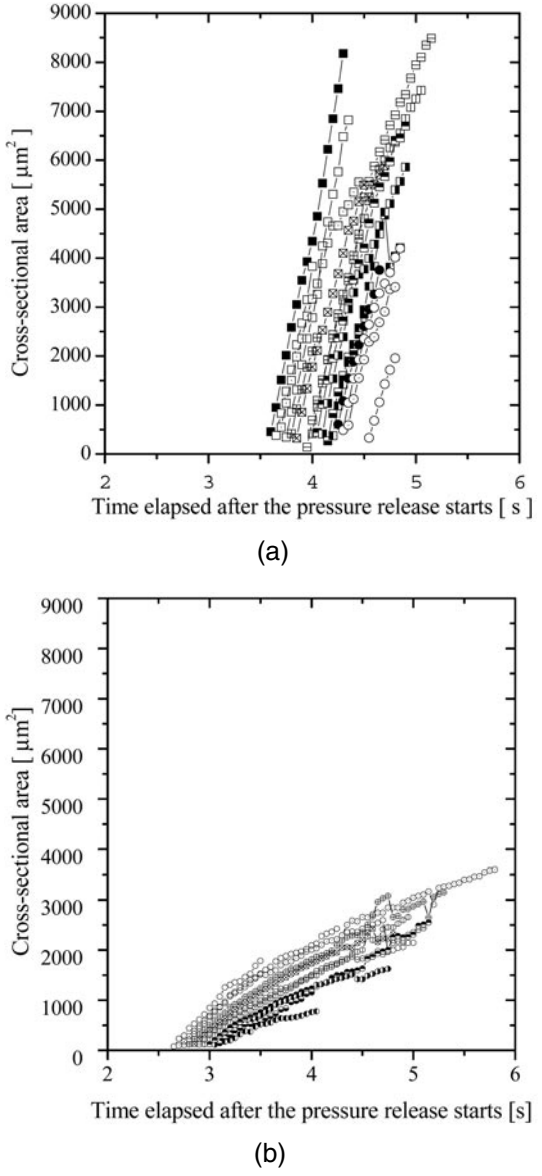

Fig. 7. Change in cross-sectional area of bubble at (a) PPMA foaming and (b) PPCN7.5 foaming.

CO_2 from the matrix polymer to bubbles as well as the viscoelasticity of the polymer. When the mass transfer primarily determines the bubble growth rate, the change in bubble radius is proportional to square root of time (18, 23), which is equivalent to the change in the cross-sectional area of the bubbles being proportional to time. Therefore, *Figs. 7a* and *b* indicate that the bubble growth at the early stage of both PPMA and composite foaming is a mass transfer–controlled process (diffusion-controlled process).

Comparing *Figs. 7a* with *b*, it can be found that the bubble growth rate at the PPCN7.5 foaming is lower than that at the PPMA foaming. *Figure 8* shows the representative growth rate of the bubbles born at the designated time in PPMA and composite foaming. The error bar indicates the standard deviation of the representative average growth rate of bubbles born at the same time. As shown in *Fig. 8*, the bubble growth rate decreases with the increase of clay content. Since the change in the cross-sectional area of the bubbles can be approximated by a linear function of time as described previously, the bubble growth observed by micrographs is a mass transfer–controlled process. Therefore, it can be said that the clay content changes the mass transfer rate of CO_2 from the matrix polymer to the bubbles.

Diffusion coefficients were also measured from the temporal change in weight of the sample under the pressurized CO_2. The measurements were performed by stepwise changing the pressure of CO_2 by 2 MPa. In *Fig. 9*, the diffusion coefficients into PPMA and composites are plotted against pressure. In general, when CO_2 dissolves in a polymer, it swells the polymer. The diffusivity of CO_2 is increased by the free volume expansion caused by the CO_2 dissolution. In this study, however, the effect of swelling on diffusivity, i.e., the concentration-dependence of the diffusion coefficient, is small for all samples, as illustrated in *Fig. 9*. At any pressure level, the diffusion coefficient of CO_2 decreases as clay content increases. This result agrees with the fact that the gas permeability of the nanocomposites decreases as the weight fraction of clay increases (9, 10).

As can be seen in *Figs. 6* and *9*, the clay reduces the diffusivity of CO_2 while keeping the solubility of CO_2 in the matrix polymer the same. Namely, owing to the clay-induced diffusivity depression, the increase in clay content depresses the mass transfer of CO_2 from the matrix polymer to the bubbles. As a result, the bubble growth rate is decreased.

Another factor affecting the mass transfer of CO_2 is the concentration of CO_2 in the matrix polymer. The solubility data illustrated in *Fig. 6* indicates that as long as the saturation pressure is kept at the same value, the clay content does not affect the concentrations of CO_2 in the matrix polymer at steady state. However, when the number of nucleated bubbles is larger, the amount of consumption of CO_2 for nucleating the bubbles becomes larger and the amount of CO_2 remaining in the matrix polymer is lower. Consequently, when the number of bubbles increases, the concentration of CO_2 in the matrix polymer dynamically reduces and the mass transfer rate of CO_2 from the matrix polymer to bubbles is depressed. In fact, as illustrated in *Fig. 7b*, the representative average growth rate decreases gradually as time elapses.

CONCLUSIONS

Polypropylene-clay nanocomposites were foamed by CO_2. Using a visual observation apparatus, we observed the effect of clay on bubble nucleation and growth rates *in situ*. And by employing some image-processing techniques, we quantitatively analyzed the bubble nucleation rate and bubble growth rate. The observation revealed that the number density of bubbles in composite increases and the bubble growth rate decreases as the

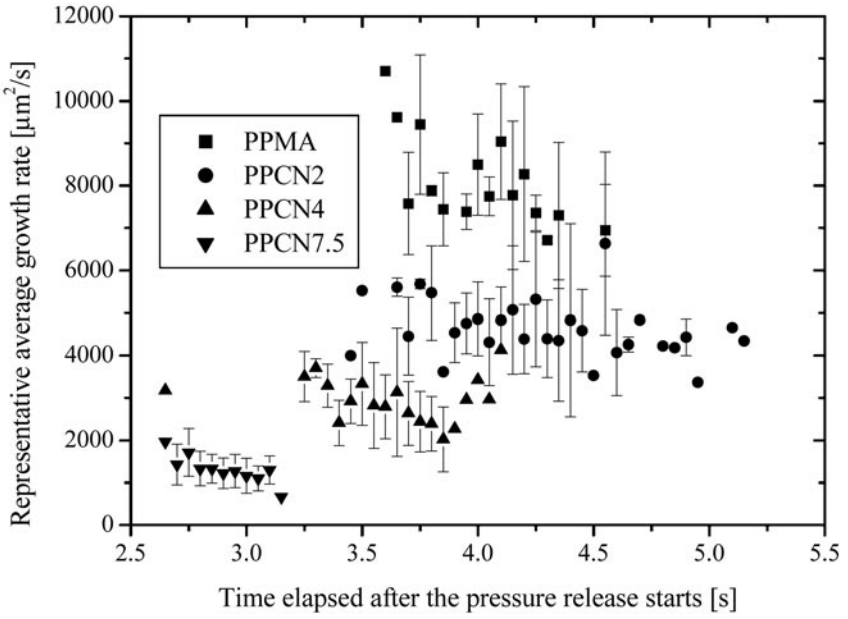

Fig. 8. Representative average growth rates for PPMA and composite foaming.

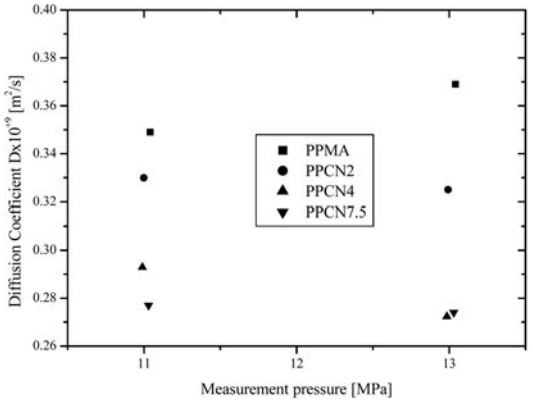

Fig. 9. Diffusion coefficient of CO_2 into PPMA and composites.

clay content increases. The clay acts as a nucleating agent and enhances bubble nucleation. The presence of the clay in the composite decreases the diffusivity of CO_2, while it does not affect the solubility in the matrix polymer. In the foaming process, the mass transfer of CO_2 from matrix to bubble is affected by the clay in two ways: diffusivity of CO_2 in composites is reduced, and the concentration of CO_2 in the matrix polymer is greatly reduced in the course of foaming because of the enhancement of nucleation by the clay.

The dynamic behavior of bubble growth in the early stage of composite foaming can be regarded as a diffusion-controlled process. In other words, viscosity does not affect the bubble growth rate in the early stage of foaming. However, when the pressure difference between the inside bubble and surrounding polymer is larger, which occurs at the initial stage of bubble growth, the viscosity could predominantly determine the growth rate.

ACKNOWLEDGMENT

Dr. Katsuto Ohtake, National Institute of Advanced Industrial Science and Technology, Japan, is greatly acknowledged for providing a design of the batch visual observation cell.

REFERENCES

1. M. Kawasumi, N. Hasegawa, M. Kato, A. Usuki, and A. Okada, *Macromolecules*, **30(20)**, 6333–38 (1997).
2. M. Okamoto, P. H. Nam, P. Maiti, and T. Kotaka, *Nanoletter*, **1**, 295 (2001).
3. P. H. Nam, P. Matti, M. Okamoto, T. Kotaka, N. Hasegawa, and A. Usuki, *Polymer*, **42**, 9633–40 (2001).
4. SS. Ray, K. Yamada, A. Ogami, M. Okamoto, and K. Ueda, *Macromol. Rapid Commun.*, **23**, 943–47 (2002).
5. K. H. Wang, M. H. Choi, C. M. Koo, Y. S. Choi, and I. J. Chung, *Polymer*, **42**, 9819–26 (2001).
6. P. Svoboda, C. Zeng, H. Wang, L. J. Lee, and D. L. Tomasko, *J. Appl. Polym. Sci.*, **85**, 1562–70 (2002).
7. T. H. Kim, S. T. Lim, C. H. Lee, H. J. Choi, and M. S. Jhon, *J. Appl. Polym. Sci.*, **87**, 2106–12 (2003).
8. C. M. Koo, M. J. Kim, M. H. Choi, S. O. Kim, and I. J. Chung, *J. Appl. Polym. Sci.*, **88**, 1526–35 (2003).
9. P. B. Messersmith and E. P. Giannelis, *J. Polym. Sci. Part A: Polym. Chem.*, **33(7)**, 1047–57 (1995).
10. J. C. Matayabas and S. R. Turner, *Polymer-Clay Nanocomposites*, pp. 207–26, T. J. Pinnavaia and G. W. Beall, eds., John Wiley & Sons, Ltd. (2000).
11. J. W. Gilman, C. L. Jackson, A. B. Morgan, R. Harris, E. Manias, E. P. Giannelis, M. Wuthenow, D. Hilton, and S. H. Phillips, *Chem. Mater.*, **12**, 1866–73 (2000).
12. J. E. Martini, Ph.D. Thesis, Massachusetts Institute of Technology (1981).
13. D. I. Collias and D. G. Baird, *Polym. Eng. Sci.*, **35**, 1167 (1995).
14. D. I. Collias and D. G. Baird, *Polym. Eng. Sci.*, **35**, 1179 (1995).
15. P. H. Nam, P. Maiti, M. Okamoto, T. Kotaka, T. Nakayama, M. Takada, M. Ohshima, A. Usuki, N. Hasegawa, and H. Okamoto, *Polym. Eng. Sci.*, **42**, 1907 (2002).
16. M. Mitsunaga, Y. Ito, SS. Ray, M. Okamoto, and K. Hironaka, *Macromol. Mater. Eng.*, **288**, 543–48 (2003).

17. Y. Fujimoto, SS. Ray, M. Okamoto, A. Ogami, K. Yamada, and K. Ueda, *Macromol. Rapid Commun.*, **24**, 457–61 (2003).
18. K. Taki, T. Nakayama, T. Yatsuzuka, and M. Ohshima, *J. Cellular Plastics*, **39**, 2, 155–68 (2003).
19. S. Areerat, Y. Hayata, R. Katsumoto, T. Kegasawa, H. Egami, and M. Ohshima, *J. Appl. Polym. Sci.*, **86**, 282–88 (2002).
20. I. C. Sanchez and R. H. Lacombe, *J. Phys. Chem.*, **80**, 2352–62 (1976).
21. R. H. Lacombe and I. C. Sanchez, *J. Phys. Chem.*, **80**, 2568–80 (1976).
22. I. C. Sanchez and R. H. Lacombe, *Macromolecules*, **11**, 1145–56 (1978).
23. D. Venerus, *Polym. Eng. Sci.*, **41**, 1390 (2001).